Transversal light forces in semiconductors

2003 J. Phys.: Condens. Matter 15 1119

(http://iopscience.iop.org/0953-8984/15/7/309)

INSTITUTE OF PHYSICS PUBLISHING JOURNAL OF PHYSICS: CONDENSED MATTER

J. Phys.: Condens. Matter **15** (2003) 1119–1135 PII: S0953-8984(03)56961-2

Transversal light forces in semiconductors

M Lindberg[1] **and R Binder**[2]

[1] Institutionen för Fysik, Åbo Akademi, Porthansgatan 3, 20500 Åbo, Finland
[2] Optical Sciences Center, University of Arizona, Tucson, AZ 85721, USA

Received 29 November 2002
Published 10 February 2003
Online at stacks.iop.org/JPhysCM/15/1119

Abstract

The transversal light force is a well established effect in atomic and molecular systems that are exposed to spatially inhomogeneous light fields. In this paper it is shown theoretically that in an excited semiconductor, containing an electron–hole plasma or excitons, a similar light force exists, if the semiconductor is exposed to an ultrashort spatially inhomogeneous light field. The analysis is based on the equations of motion for the Wigner distribution functions of charge carrier populations and interband polarizations. The results show that, while the light force on the electron–hole plasma or the excitons does exist, its effects on the kinetic behaviour of the electron–hole plasma or the excitons are different compared to the situation in an atomic or molecular system. A detailed analysis presented here traces this difference back to the principal differences between atoms and molecules on the one hand and electron–hole plasmas or excitons on the other hand.

1. Introduction

In recent years research has revealed that there exists a close analogy between semiconductors and atoms. Experiments have verified that e.g. photon echoes, optical Stark shift and Rabi floppings well established in atomic systems can also be observed in semiconductor experiments (see, e.g., [1–14] and for a comprehensive review [15]). It has been shown that strong light beams can cause changes in the mechanical state of atoms, making it possible e.g. to cool down the centre of mass motion of atoms. In the case of atomic samples the light forces have played an important role e.g. in creation of Bose–Einstein condensates of atoms. A possible Bose–Einstein condensation of excitons is still an interesting question and would benefit from new experimental tools. In this paper we study one such mechanical phenomenon, the transversal light force, in semiconductors. It would be of great practical interest if corresponding mechanical manipulations, as with atoms, even in some form were possible with charge carriers or excitons in a semiconductor.

The transversal light force, originally proposed by Ashkin [16], has been shown to exist when atoms are illuminated with an off-resonant light field with a transversal spatial intensity profile. Experiments have shown that the force in the case of atoms is strong enough to move

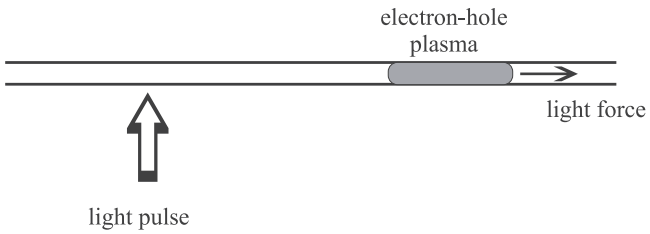

Figure 1. Schematic figure of the light force geometry with an initial electron–hole plasma in a (one-dimensional) semiconductor.

atoms around. Several reviews of the progress in this field have already been written [17–19]. It has also been shown that the same principle functions with dielectric spheres or even with bacteria. Analogously, a spatially inhomogeneous carrier distribution in semiconductors also represents a spatially inhomogeneous change in the dielectric properties relative to the background dielectric constant and should therefore experience a force when a spatially inhomogeneous light field profile is present.

In this paper we concentrate on demonstrating theoretically that semiconductor carrier systems experience the same kinds of transversal mechanical force as atoms do. The basic geometry is shown schematically in figure 1. The starting point of our theory is an inhomogeneous representation of equations of motion for the one-particle expectation values. Essentially the same basic equations, even including the Coulomb effects, have been derived earlier using Green function techniques in [20, 21]. In those works, however, the solutions of the equations were not thoroughly analysed. The consequences of the spatial inhomogeneity have been studied e.g. in the problem of light propagation in thick quantum wells [22]. The authors solve the equations of motion in order to study the coupled dynamics of a light beam and the carriers it creates. The goal of our work is to analyse how far the analogy between semiconductors and atoms carries in the case of phenomena that have their origin in the inhomogeneity of the material. Starting with the Hamiltonian for free carriers interacting with the light field we derive the general spatially inhomogeneous equations of motion. Consequently, a Boltzmann-type equation of motion is derived for the position–momentum distribution function of the carriers. From that equation we can identify the transverse light force. We show that a semiconductor carrier system absorbs transverse momentum from a light beam if the beam has a transverse intensity profile. It will be a challenging task to observe directly the corresponding motion of the spatial distribution of the carriers. We also show that when momentum is absorbed leading to motion of the carrier distributions there is no electric current linear in intensity of the light field if no dephasing or scattering of the carriers takes place. A net current in higher order in intensity is, however, not excluded. Analytical results are represented with corresponding numerical evaluations in a 1D approximation.

2. Model and basic definitions

We model the semiconductor as a two-band system with parabolic bands in order to demonstrate the principles. A more physically correct band structure is straightforward to include if practical calculations are made. The most serious approximation we make is neglecting the Coulomb effects everywhere except in the weak field limit. It is obvious that with this approximation we cannot expect quantitative results but we do not expect the Coulomb interaction to strongly modify the principle of the process. The Coulomb interaction conserves the total momentum

of the carrier system and does not, therefore, modify the momentum already absorbed by the carrier system. Only redistribution between the carriers is expected. We treat all decay and dephasing processes phenomenologically in order to keep the treatment simple and transparent.

Our model many-body Hamiltonian $\hat{H}$ in the spatial representation is given by

$$\hat{H} = \Delta \int \mathrm{d}\vec{r}\, \Psi_e^\dagger(\vec{r})\Psi_e(\vec{r}) - \frac{\hbar}{2m_e}\int \mathrm{d}\vec{r}\, \Psi_e^\dagger(\vec{r})\nabla^2\Psi_e(\vec{r}) - \frac{\hbar}{2m_h}\int \mathrm{d}\vec{r}\, \Psi_h^\dagger(\vec{r})\nabla^2\Psi_h(\vec{r}) - \int \mathrm{d}\vec{r}\, \vec{\mu}\cdot\vec{E}(\vec{r})\Psi_e^\dagger(\vec{r})\Psi_h^\dagger(\vec{r}) - \int \mathrm{d}\vec{r}\, \vec{\mu}\cdot\vec{E}^*(\vec{r})\Psi_h(\vec{r})\Psi_e(\vec{r}) \tag{1}$$

where Δ is the detuning from the band edge. For consistent units $\vec{\mu}$ is equal to the dipole moment divided by $\hbar$. The rotating wave approximation is assumed and the fast frequency removed. The interaction with the light field is taken in the local dipole approximation where we have assumed that the wavelength of the light is much larger than the size of the unit cell.

When transformed into the momentum representation the Hamiltonian takes the form

$$\hat{H} = \Delta\sum_{\vec{k}} \Phi_e^\dagger(\vec{k})\Phi_e(\vec{k}) + \frac{\hbar}{2m_e}\sum_{\vec{k}} \vec{k}^2\Phi_e^\dagger(\vec{k})\Phi_e(\vec{k}) + \frac{\hbar}{2m_h}\sum_{\vec{k}} \vec{k}^2\Phi_h^\dagger(\vec{k})\Phi_h(\vec{k}) - \sum_{\vec{k}\vec{k}'} \vec{\mu}\cdot\tilde{\vec{E}}(\vec{k}+\vec{k}')\Phi_e^\dagger(\vec{k})\Phi_h^\dagger(\vec{k}') - \sum_{\vec{k}\vec{k}'} \vec{\mu}\cdot\tilde{\vec{E}}^*(\vec{k}+\vec{k}')\Phi_h(\vec{k}')\Phi_e(\vec{k}) \tag{2}$$

where

$$\vec{\mu}\cdot\tilde{\vec{E}}(\vec{k}) \equiv \frac{1}{V}\int \mathrm{d}\vec{r}\, \vec{\mu}\cdot\vec{E}(\vec{r})\mathrm{e}^{-\mathrm{i}\vec{k}\cdot\vec{r}}. \tag{3}$$

The relation between the field operators in the different representations is given by

$$\begin{aligned}\Psi(\vec{r}) &= \frac{1}{\sqrt{V}}\sum_{\vec{k}} \Phi(\vec{k})\mathrm{e}^{\mathrm{i}\vec{k}\cdot\vec{r}}\\ \Phi(\vec{k}) &= \frac{1}{\sqrt{V}}\int \mathrm{d}\vec{r}\, \Psi(\vec{r})\mathrm{e}^{-\mathrm{i}\vec{k}\cdot\vec{r}}.\end{aligned} \tag{4}$$

The total momenta $\hat{\vec{P}}_e$ and $\hat{\vec{P}}_h$ of the carriers are simplest in the momentum representation and are given by

$$\hat{\vec{P}}_{e,h} = \sum_{\vec{k}} \hbar\vec{k}\Phi_{e,h}^\dagger(\vec{k})\Phi_{e,h}(\vec{k}). \tag{5}$$

The total momentum is then given by $\hat{\vec{P}} = \hat{\vec{P}}_e + \hat{\vec{P}}_h$. One must, however, notice that the corresponding current density operators $\hat{\vec{J}}_e$ and $\hat{\vec{J}}_h$ are not directly given by the total momentum because they are related to the velocity of the carrier system. For parabolic bands we obtain the relations

$$\hat{\vec{J}}_{e,h} = -\frac{q_{e,h}}{m_{e,h}}\hat{\vec{P}}_{e,h} \tag{6}$$

with $q_e = -e$ and $q_h = e$.

The closest quantum mechanical counterpart of the classical phase space distribution function is the Wigner function. Because we are only interested in the single-particle expectation values we define the single-particle Wigner function $W(\vec{R}, \vec{K})$ by

$$W(\vec{R},\vec{K}) = \sum_{\vec{q}} \mathrm{e}^{-\mathrm{i}\vec{q}\cdot\vec{R}}\langle\Phi^\dagger(\vec{K}+\vec{q}/2)\Phi(\vec{K}-\vec{q}/2)\rangle = \int \mathrm{d}\vec{r}\, \mathrm{e}^{\mathrm{i}\vec{K}\cdot\vec{r}}\langle\Psi^\dagger(\vec{R}+\vec{r}/2)\Psi(\vec{R}-\vec{r}/2)\rangle. \tag{7}$$

It is a well known fact that the Wigner function is positive definite only if it is a Gaussian. However, it gives the symmetrically ordered operator expectation values as if it were a classical distribution function. The positive definite spatial density and momentum distribution are obtained by

$$\frac{1}{V}\int \mathrm{d}\vec{R}\, W(\vec{R},\vec{K}) = \langle \Phi^{\dagger}(\vec{K})\Phi(\vec{K})\rangle \tag{8}$$

and

$$\frac{1}{V}\sum_{\vec{K}} W(\vec{R},\vec{K}) = \langle \Psi^{\dagger}(\vec{R})\Psi(\vec{R})\rangle \tag{9}$$

and the total number of carriers in a spatially confined sample is given by

$$\frac{1}{V}\sum_{\vec{K}}\int \mathrm{d}\vec{R}\, W(\vec{R},\vec{K}) = N_{tot}. \tag{10}$$

The definitions for both electrons and holes have been taken to be the same with their corresponding field operators.

For the equations of motion to be complete we also define the polarization amplitude $P(\vec{R},\vec{r})$ by

$$P(\vec{R},\vec{r}) \equiv \langle \Psi_h(\vec{R}-\vec{r}/2)\Psi_e(\vec{R}+\vec{r}/2)\rangle. \tag{11}$$

The momentum representation of the polarization is obtained using the transformations of the field operators.

3. Equations of motion

The equations of motion for the $W(\vec{R},\vec{K})$ and $P(\vec{R},\vec{r})$ are obtained directly from the Heisenberg equations of motion for the field operators. They are given by

$$\begin{aligned}\frac{\partial}{\partial t}W_{e,h}(\vec{R},\vec{K}) = {} & -\frac{\hbar}{m_{e,h}}\vec{K}\cdot\nabla_{\vec{R}}W_{e,h}(\vec{R},\vec{K}) + \mathrm{i}\int \mathrm{d}\vec{r}\,\mathrm{e}^{\mathrm{i}\vec{K}\cdot\vec{r}}\vec{\mu}\cdot\vec{E}(\vec{R}-\vec{r}/2)P^{*}(\vec{R},\sigma_{e,h}\vec{r}) \\ & -\mathrm{i}\int \mathrm{d}\vec{r}\,\mathrm{e}^{-\mathrm{i}\vec{K}\cdot\vec{r}}\vec{\mu}\cdot\vec{E}^{*}(\vec{R}-\vec{r}/2)P(\vec{R},\sigma_{e,h}\vec{r})\end{aligned} \tag{12}$$

where the index e is chosen for electrons and h for holes with $\sigma_e = +1$ and $\sigma_h = -1$ and

$$\begin{aligned}\frac{\partial}{\partial t}P(\vec{R},\vec{r}) = {} & (-\mathrm{i}\Delta-\gamma)P(\vec{R},\vec{r}) + \mathrm{i}\left(\frac{\hbar}{2m_e}+\frac{\hbar}{2m_h}\right)\left(\frac{1}{4}\nabla^2_{\vec{R}}+\nabla^2_{\vec{r}}\right)P(\vec{R},\vec{r}) \\ & +\mathrm{i}\left(\frac{\hbar}{2m_e}-\frac{\hbar}{2m_h}\right)\nabla_{\vec{R}}\cdot\nabla_{\vec{r}}P(\vec{R},\vec{r}) + \mathrm{i}\vec{\mu}\cdot\vec{E}(\vec{R})\delta(\vec{r}) \\ & -\mathrm{i}\vec{\mu}\cdot\vec{E}(\vec{R}-\vec{r}/2)\frac{1}{V}\sum_{\vec{K}'}W_e(\vec{R},\vec{K}')\mathrm{e}^{\mathrm{i}\vec{K}'\cdot\vec{r}} \\ & -\mathrm{i}\vec{\mu}\cdot\vec{E}(\vec{R}+\vec{r}/2)\frac{1}{V}\sum_{\vec{K}'}W_h(\vec{R},\vec{K}')\mathrm{e}^{-\mathrm{i}\vec{K}'\cdot\vec{r}}.\end{aligned} \tag{13}$$

We have added a phenomenological dephasing rate to the equation to approximate the physical dephasing processes which for semiconductors can hardly ever be completely neglected. In the limit where Wigner functions are assumed to be slowly varying functions of their variables we can make a gradient expansion for the field amplitude neglecting

all derivatives of order two or higher. We introduce the polarization Wigner function $P(\vec{R}, \vec{K}) \equiv \int \mathrm{d}\vec{r}\, \mathrm{e}^{-\mathrm{i}\vec{K}\cdot\vec{r}} P(\vec{R}, \vec{r})$. This gives us the equations of motion in the form

$$\begin{aligned}\frac{\partial}{\partial t} W_{e,h}(\vec{R}, \vec{K}) = &-\frac{\hbar}{m_{e,h}} \vec{K} \cdot \nabla_{\vec{R}} W_{e,h}(\vec{R}, \vec{K}) + \mathrm{i}(\vec{\mu} \cdot \vec{E}(\vec{R}) P^*(\vec{R}, \sigma_{e,h}\vec{K}) \\ &- \vec{\mu} \cdot \vec{E}^*(\vec{R}) P(\vec{R}, \sigma_{e,h}\vec{K})) - \tfrac{1}{2}(\nabla_{\vec{R}}(\vec{\mu} \cdot \vec{E}(\vec{R})) \cdot \nabla_{\vec{K}} P^*(\vec{R}, \sigma_{e,h}\vec{K}) \\ &+ \nabla_{\vec{R}}(\vec{\mu} \cdot \vec{E}^*(\vec{R})) \cdot \nabla_{\vec{K}} P(\vec{R}, \sigma_{e,h}\vec{K})) \end{aligned} \tag{14}$$

and

$$\begin{aligned}\frac{\partial}{\partial t} P(\vec{R}, \vec{K}) = &(-\mathrm{i}\Delta - \gamma) P(\vec{R}, \vec{K}) + \mathrm{i}\left(\frac{\hbar}{2m_e} + \frac{\hbar}{2m_h}\right)\left(\frac{1}{4}\nabla^2_{\vec{R}} - \vec{K}^2\right) P(\vec{R}, \vec{K}) \\ &- \left(\frac{\hbar}{2m_e} - \frac{\hbar}{2m_h}\right) \vec{K} \cdot \nabla_{\vec{R}} P(\vec{R}, \vec{K}) + \mathrm{i}\vec{\mu} \cdot \vec{E}(\vec{R})(1 - W_e(\vec{R}, \vec{K}) \\ &- W_h(\vec{R}, -\vec{K})) - \tfrac{1}{2}\nabla_{\vec{R}}(\vec{\mu} \cdot \vec{E}(\vec{R})) \cdot \nabla_{\vec{K}}(W_e(\vec{R}, \vec{K}) - W_h(\vec{R}, -\vec{K})). \end{aligned} \tag{15}$$

We shall use equations (14) and (15) in numerics; however, we obtain more insight if we assume that the pulses are long enough to warrant the adiabatic elimination of the polarization. We also neglect the spatial derivatives of the polarization Wigner function. This gives us the polarization Wigner functions in the form

$$\begin{aligned}P(\vec{R}, \vec{K}) \approx &\left(\gamma + \mathrm{i}\left(\Delta + \left(\frac{\hbar}{2m_e} + \frac{\hbar}{2m_h}\right)\vec{K}^2\right)\right)^{-1} (+\mathrm{i}\vec{\mu} \cdot \vec{E}(\vec{R})(1 - W_e(\vec{R}, \vec{K}) \\ &- W_h(\vec{R}, -\vec{K})) - \tfrac{1}{2}\nabla_{\vec{R}}(\vec{\mu} \cdot \vec{E}(\vec{R})) \cdot \nabla_{\vec{K}}(W_e(\vec{R}, \vec{K}) - W_h(\vec{R}, -\vec{K}))). \end{aligned} \tag{16}$$

Inserting the polarization Wigner function into the equations of motion for the Wigner functions we obtain

$$\begin{aligned}\frac{\partial}{\partial t} W_{e,h}(\vec{R}, \vec{K}) = &-\frac{\hbar}{m_{e,h}} \vec{K} \cdot \nabla_{\vec{R}} W_{e,h}(\vec{R}, \vec{K}) \\ &+ \nabla_{\vec{R}}(|\vec{\mu} \cdot \vec{E}(\vec{R})|^2) \cdot \nabla_{\vec{K}}\left(\frac{\Delta(\vec{K})}{\gamma^2 + \Delta(\vec{K})^2} W_{e,h}(\vec{R}, \vec{K})\right) \\ &- \mathrm{Im}(\vec{\mu} \cdot \vec{E}(\vec{R}) \nabla_{\vec{R}}(\vec{\mu} \cdot \vec{E}^*(\vec{R})) \cdot \nabla_{\vec{K}}\left(\frac{\gamma}{\gamma^2 + \Delta(\vec{K})^2} W_{h,e}(\vec{R}, -\vec{K})\right) \\ &+ |\vec{\mu} \cdot \vec{E}(\vec{R})|^2 \frac{2\gamma}{\gamma^2 + \Delta(\vec{K})^2}(1 - W_{e,h}(\vec{R}, \vec{K}) - W_{h,e}(\vec{R}, -\vec{K})) \end{aligned} \tag{17}$$

where $\Delta(\vec{K}) \equiv \Delta + (\frac{\hbar}{2m_e} + \frac{\hbar}{2m_h})\vec{K}^2$. One of the equations is obtained by choosing the first indices and the second equation by choosing the second indices. We have assumed the $\vec{K}$-gradients of the Lorentzians to be small and they have been neglected. The equations obtained have a form very similar to the Liouville equation for classical distribution functions. The first term on the right-hand side is the convective derivative connecting momentum and change of position. The second and third terms are the force terms displaying explicitly the light force applied to the carriers. The forces contain a longitudinal and a transversal part. In this paper we only discuss the transversal part of the force neglecting completely the longitudinal dimension of the equation represented by the third term. This is a reasonable and often used approximation in quantum wells under normal light incidence conditions. The multiplying function in the second term gives the transversal light force $\vec{F}_{transv}(\vec{R})$, also called the dispersive light force. It is given by the expression

$$\vec{F}_{transv}(\vec{R}) = -\hbar \nabla_{\vec{R}}(|\vec{\mu} \cdot \vec{E}(\vec{R})|^2) \frac{\Delta(\vec{K})}{\gamma^2 + \Delta(\vec{K})^2}. \tag{18}$$

This is the same expression as is obtained in the case of atoms below saturation. In addition, the equation of motion has an extra term, the fourth one, a source term due to the optical creation of carriers by absorption of light. It differs from its atomic counterpart in that it does not limit the total number of carriers created, whereas in the atomic case the number of atoms is fixed. A fundamental difference between semiconductors and atoms is that the light beam always creates new carriers in a semiconductor whereas in a gas the number of atoms is not changed by the interaction with light.

Another difference is present too: the sign of the force is opposite to the atomic case. The force is repulsive for detunings below resonance, whereas for atoms it is attractive. In atoms the interaction starts from an internal ground state combined with a centre of mass state with kinetic energy. When the atom interacts with a field with below resonance frequency it gives up kinetic energy in order to fill the energy gap, and consequently it is decelerated. Hence, the force is attractive. In a semiconductor the ground state is the vacuum, which does not contain free kinetic energy to spare. The electron–hole pairs have to be created before they can interact with the light field. Once the pairs have been created the semiconductor system is in an excited state with possible extra kinetic energy. When the pairs interact with the light field with a below resonance frequency they start to transfer from the excited state towards the vacuum state emitting into the light field. The light field frequency is, however, smaller than the frequency corresponding to the excited state, and hence part of the internal energy has to be transferred into the kinetic energy. Consequently, the pair is accelerated.

4. Numerical results

When a single light beam with a symmetric transversal intensity profile travels through a semiconductor medium the absorption will create carriers. This carrier system will not have a net total transversal momentum because of the symmetry of the situation. The situation is different if the same beam travels in the spatial neighbourhood of previously created carriers. In this situation the previously created carriers can gain net momentum even if the new carriers created by the beam itself do not. In this section we assume first an initial carrier distribution created perhaps by an earlier pulse. A light beam with a transversal intensity profile is provided close to the carriers.

In order to analyse the momentum transfer and to discuss the related physical processes in detail, we have performed numerical calculations in one dimension. We assumed that spatially inhomogeneous and incoherent distributions of electrons and holes had been created before a light pulse was applied. The initial electron and hole distributions were assumed to be of Gaussian shape and had initially spatial FWHM of 2 μm and momentum FWHM of 2×10^{-2} Å^{-1}. The maximum values were set equal to $w_{e0} = w_{h0} = 0.6$. The light pulse was taken to last 2.0 ps (FWHM of the intensity) and its maximum amplitude was equal to 40 meV. The integration was started 6.01 ps before the pulse maximum. The transversal width was chosen to be 2 μm. Its detuning was 40 meV below the band edge. The transversal distance between the maxima of the initial carrier distributions and the maximum of the light field was chosen to be 2 μm. The effective masses of the electrons and holes were taken to be 0.067 m_e and 0.197 m_e, respectively, the Bohr radius a_0 was 100 Å and the background dielectric constant ϵ_r was 12.7.

The equations (14) and (15) were solved using a Runge–Kutta method and both spatial and momentum distributions were evaluated. Using equations (14) and (15) instead of equation (17) allowed us to eliminate one possible error source, namely the assumption of adiabatic following, but the final results were not dramatically different. In figure 2(a) we show the momentum distributions $W_e(\vec{R}, \vec{K})$ and $W_h(\vec{R}, -\vec{K})$ (integrated over $\vec{R}$) before and after the pulse in the

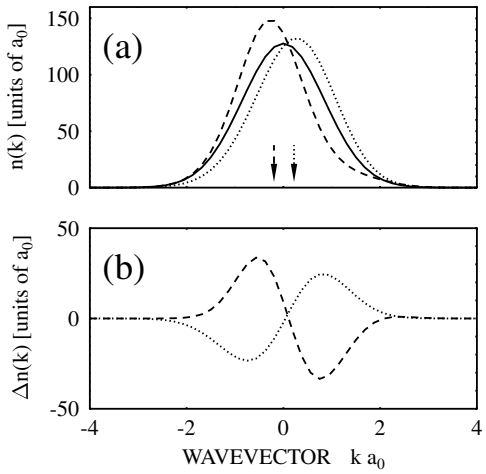

Figure 2. (a) Momentum distributions $W_e(\vec{R}, \vec{K})$ and $W_h(\vec{R}, -\vec{K})$ (integrated over $\vec{R}$) before ($t = -6$ ps) and after ($t = +4$ ps) the pulse. Before the pulse, the electron and hole distributions are identical (solid curve). After the pulse, the electron distribution is shown as the dashed curve, and the hole distribution as the dotted curve. The arrows indicate the wavevector per particle for the electrons (dashed arrow) and holes (dotted arrow) after the pulse. (b) The difference of the distribution after and before the pulse for electrons (dashed curve) and holes (dotted curve). All results shown in this figure are computed with zero dephasing, $\gamma = 0$. The Bohr radius a_0 is chosen to be 100 Å.

case when the dephasing γ is set equal to zero, which is called the coherent approximation. This is clearly an unphysical situation but it demonstrates the most ideal situation and its results can be used as a reference for the cases with more realistic γ-values. We want as few additional carriers as possible to be present after the pulse because those would mask the effect of the light force. When the pulse is highly detuned as in our case the pulse spectrum does not have any considerable overlap with the resonance. The Gaussian temporal envelope relates to a Gaussian frequency spectrum with a width which is clearly smaller than the detuning. In this case the pulse creates carriers while it is present but the created populations adiabatically follow the temporal shape of the pulse. When the pulse has disappeared the temporally created carriers also have disappeared almost completely. The number of new carriers left behind is related to the overlap of the frequency spectrum with the resonance. The density of the temporal carriers depends on the temporal pulse intensity and can be relatively large at the pulse maximum. If the dephasing rate is not equal to zero a larger part of the temporal carriers are left after the pulse is over. Because in our case there is essentially no absorption as $\gamma = 0$ and the detuning is large, all changes in the original momentum distribution after the pulse are caused by the transversal light force while the pulse was present. We see that a clear asymmetry is created in the momentum distributions of both electrons and holes. The arrows show the position of the average momentum per particle. In order to make the change even clearer we also show in figure 2(b) the change of the momentum distributions observed after the pulse. They clearly have dispersive shapes with characteristic widths of the order of one over the Bohr radius. The net momenta per particle created for electrons and holes are indicated by arrows in figure 2(a).

The deformation of the carrier distribution is shown in figure 3 where the spatial distribution functions are shown before, during and after the pulse. During the pulse there is again an excess of carriers in the location where the light pulse propagates. After the pulse these carriers have disappeared and in the end the shape of the carrier distribution has essentially broadened.

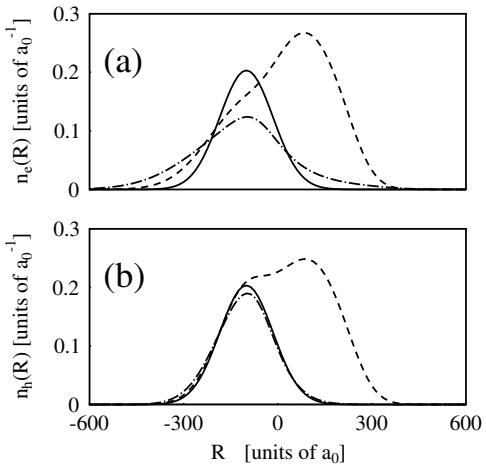

Figure 3. Spatial distributions $W_e(\vec{R}, \vec{K})$ and $W_h(\vec{R}, -\vec{K})$ (integrated over $\vec{K}$) before ($t = -6$ ps, solid curve), during ($t = 0$ ps, dashed curve) and after ($t = +4$ ps, dash–dotted curve) the pulse for electrons (a) and holes (b), following from the same calculation as used in figure 2.

The broadening is a result of the ballistic motion of the particles and would also take place without the light pulse present. However, when one studies the figure carefully one sees that the carrier distribution has also become slightly asymmetric. The effect is more pronounced for the electrons because of their smaller mass. The asymmetry is a result of the transversal light force.

In order to show what happens during the pulse we plot in figure 4(a) the total number of carriers as a function of time. Because we are in the regime of adiabatic following there is a considerable excess of carriers during the pulse, which then disappear when the pulse leaves the sample. The same temporarily present carriers show up in figure 4(c) where the centres of masses of the spatial distributions are shown as functions of time. The figure shows clearly that the distributions are no longer centred at $-100\ a_0$ as they were before the pulse. The upper of the small insets shows the uncut figure and the lower one shows the widths of the distributions as a function of time displaying the sum effect of the adiabatic creation and the ballistic broadening. The temporal behaviours of the average momenta are shown in figure 4(b). We see that the adiabatically created carriers do not gain net momentum but their temporary presence is felt in the width of the momentum distribution as is displayed by the inset.

In figures 5–7 we show the same distributions as in figures 2–4 but now with $\gamma = 0.1$ meV corresponding to a dephasing time equal to 6.6 ps. The changes in the momentum distributions are larger as shown in figure 5(b). Its shape is no longer only dispersive but also has an asymmetric back ground contribution. The reason is absorption which causes creation of new carriers which do not disappear after the pulse. The new carriers do not bring in net momentum and therefore the average momentum per particle, again shown by the arrows in figure 5(a), is smaller than in the case with no absorption.

The time development of the total population shown in figure 7(a) again shows a considerable number of carriers during the pulse but now some of them remain after the pulse has vanished, leading to a net increase of carriers as expected. The same behaviour is demonstrated in figure 6 where the development of the spatial distributions is shown. The result is a superposition of the broadened initial distribution and the distribution of the new, created carriers which follow the spatial shape of the pulse. The same dynamics is displayed

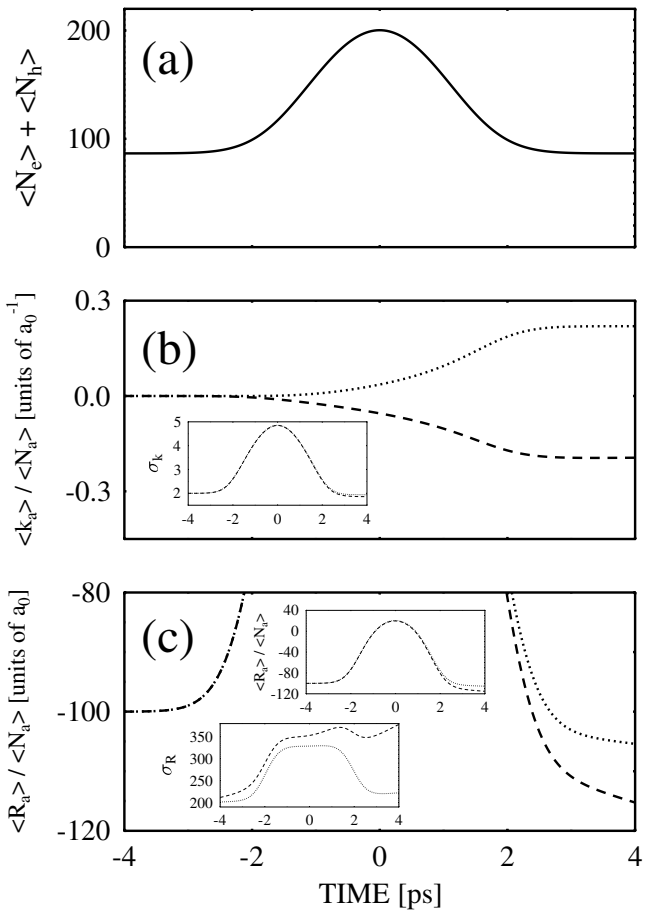

Figure 4. (a) Temporal evolution of the total particle number. (b) Temporal evolution of the wavevector per particle for electrons (dashed curve) and holes (dotted curve). The inset shows the variance (=width) of the corresponding momentum distributions in units of a_0^{-1}. (c) Temporal evolution of the spatial expectation value for electrons (dashed curve) and holes (dotted curve). During the pulse, the expectation values differ significantly from their initial value, -100 Å, since the pulse is centred at +100 Å. The full evolution is shown in the upper inset. The lower inset shows the variance (=width) of the corresponding spatial distributions in units of a_0. The results in this figure follow from the same calculation as used in figure 2.

in the time developments of the centres of mass and the average momenta. The centres of mass have gained substantial shifts which essentially all come from the creation of new carriers by absorption. The effect of the transversal light force is strongly masked.

In figures 8–10 we study the situation with two spatially separate weak pulses and no initial carrier distribution. Both pulses are assumed to have an amplitude of 0.4 meV and a detuning of -3.0 meV. The pulses are both taken to last 0.2 ps which means that their frequency spectra have a small but considerable overlap with the resonance. Hence, there will be some carriers left after the pulses even in the case of vanishing dephasing rate, $\gamma = 0$, shown in figures 8–10. The beam centred at $-100\,a_0$ arrives first and the second, centred at $100\,a_0$, comes 345 fs later. In figure 8(a) we see the momentum distribution of electrons during (solid curve) and after (dashed curve) the pulses. The momentum distribution has become narrower at the end of the

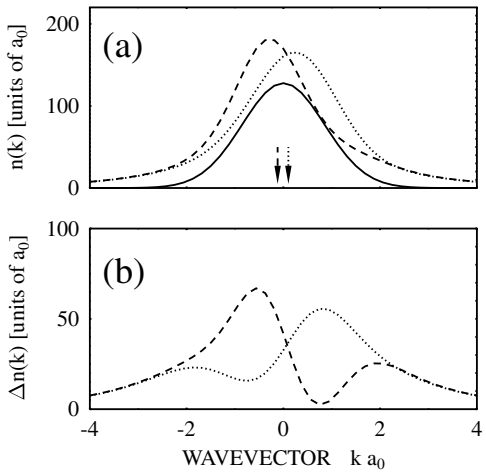

Figure 5. The same as figure 2, but for non-zero dephasing, $\hbar\gamma = 0.1$ meV.

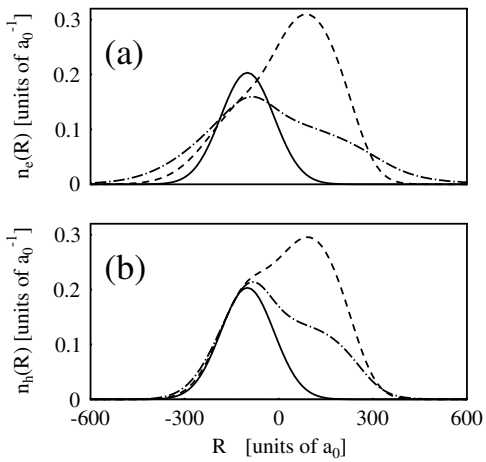

Figure 6. The same as figure 3, but for non-zero dephasing, $\hbar\gamma = 0.1$ meV.

pulses compared to that during the pulse. The difference between the electron and the hole distributions is demonstrated in figure 8(b) and it is obvious that the antisymmetric shape of the difference leads to a net total momentum. In figure 9 we see that after the pulses (dot–dashed curve) the spatial distribution of the carriers is double peaked, the peaks being situated at the centres of the beams. During the pulses the spatial distribution is asymmetric and shows that the beam centred at $-100\,a_0$ has come first. In figure 10(a) we see the time development of the total number of carriers. The two kinks in the curve show the positions where the two pulses have ended leading to a decrease in carrier generation. Even though there is no dephasing, a small number of carriers will be generated due to the overlap of the resonance and the field spectrum. In figure 10(b) we again see that the created carriers get an average momentum which is non-zero. The deviation between the shapes of the curves is created when both pulses are present. The small inset demonstrates the dynamic narrowing of the momentum distribution. Finally in figure 10(c) the centre of gravity of the spatial distribution is shown.

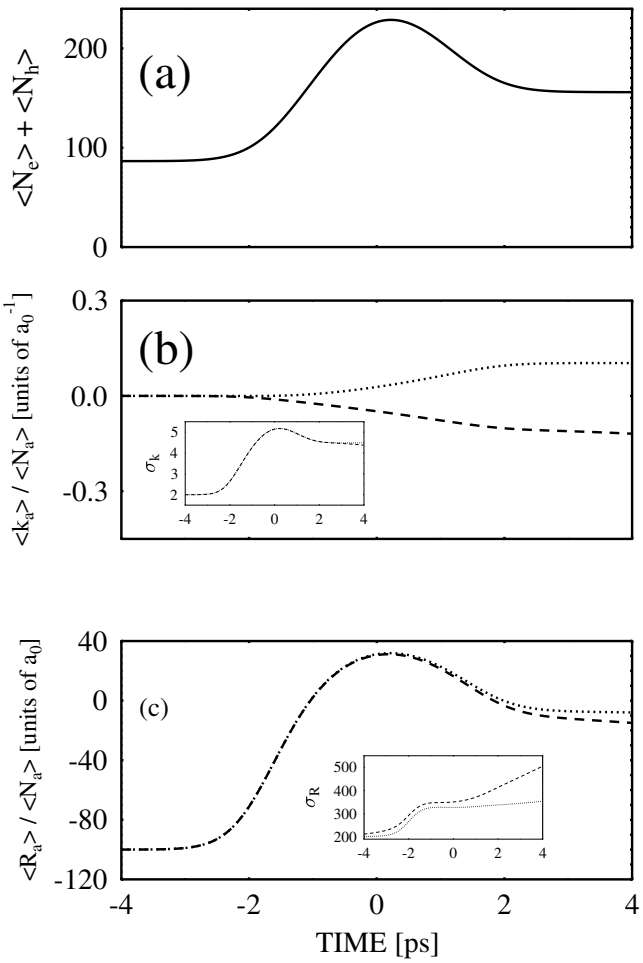

Figure 7. The same as figure 4, but for non-zero dephasing, $\hbar\gamma = 0.1$ meV.

The apparently large shift only demonstrates the creation of carriers first at $-100\ a_0$ and then an equal amount at $100\ a_0$ which leaves the centre of gravity close to zero after the pulses. The effect due to the light force is too small to be seen on the curve.

5. Discussion

5.1. Momentum transfer

In the previous section we have shown that a light beam can exert a force on an electron–hole plasma if the light and the plasma are spatially displaced. For the parameters chosen in the numerical calculation, the momentum transfer per particle was of the order of $0.1\ a_0^{-1}$ ($=10\ \mu\mathrm{m}^{-1}$). The fact that—in principle—the momentum transfer exists makes the electron–hole plasma analogous to an atom system. This is the central result of this paper. However, as we have also shown in the previous section, the light force in a semiconductor is associated with a complex kinetic behaviour of the electron–hole plasma. While atoms exposed to light forces simply move according to the acceleration brought about by the light, the electron–hole plasma suffers from broadening of the spatial width of the plasma. Moreover, the

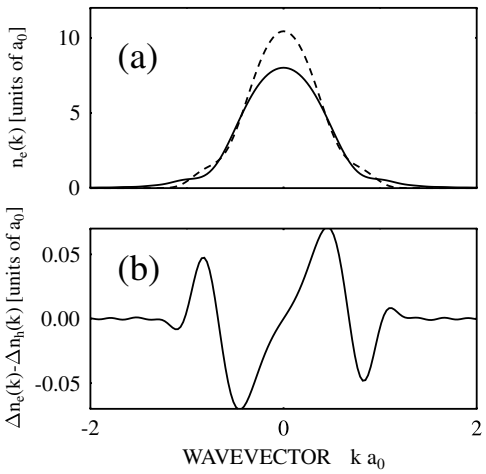

Figure 8. (a) Electron momentum distributions $W_e(\vec{R}, \vec{K})$ (integrated over $\vec{R}$) during ($t = 0$ ps, solid curve) and after ($t = +0.4$ ps, dashed curve) the second pulse, calculated for zero initial distributions within the two-pulse configuration (see text). The corresponding results for holes are indistinguishable on this plot from the ones shown. (b) The difference of the distribution after and during the pulse for electrons minus the difference of the distribution after and during the pulse for holes. All results shown in this figure are computed with zero dephasing, $\gamma = 0$.

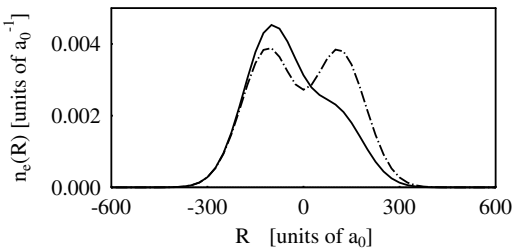

Figure 9. Spatial distribution $W_e(\vec{R}, \vec{K})$ (integrated over $\vec{K}$) during ($t = 0$ ps, solid curve), and after ($t = +0.4$ ps, dash–dotted curve) the second pulse. The results in this figure follow from the same calculation as used in figure 8. The corresponding results for holes are indistinguishable from the ones shown.

observation time of the electron–hole plasma is limited to its lifetime, and therefore the motion of the plasma can only be observed within this time frame (which, in our example of a direct-gap semiconductor, is on the order of nanoseconds). Clearly, a possible experimental observation of the plasma acceleration depends critically on the value of the momentum transfer. In order to maximize the momentum transfer, one has to understand what determines and therefore what limits the momentum transfer. We answer this question in this subsection.

We calculate the total momentum transferred to the carriers when the distribution is assumed unchanged during the process. The result for electrons is

$$\frac{\mathrm{d}}{\mathrm{d}t}\langle \vec{K}_e \rangle = -\int \mathrm{d}\vec{R}\,\frac{1}{V}\sum_{\vec{K}} \nabla_{\vec{R}}(|\vec{\mu}\cdot\vec{E}(\vec{R})|^2)\frac{\Delta(\vec{K})}{\gamma^2+\Delta(\vec{K})^2}W_e(\vec{R},\vec{K}) + \int \mathrm{d}\vec{R}\,\frac{1}{V}\sum_{\vec{K}} \vec{K}|\vec{\mu}\cdot\vec{E}(\vec{R})|^2\frac{2\gamma}{\gamma^2+\Delta(\vec{K})^2}(1-W_e(\vec{R},\vec{K})-W_h(\vec{R},-\vec{K})). \tag{19}$$

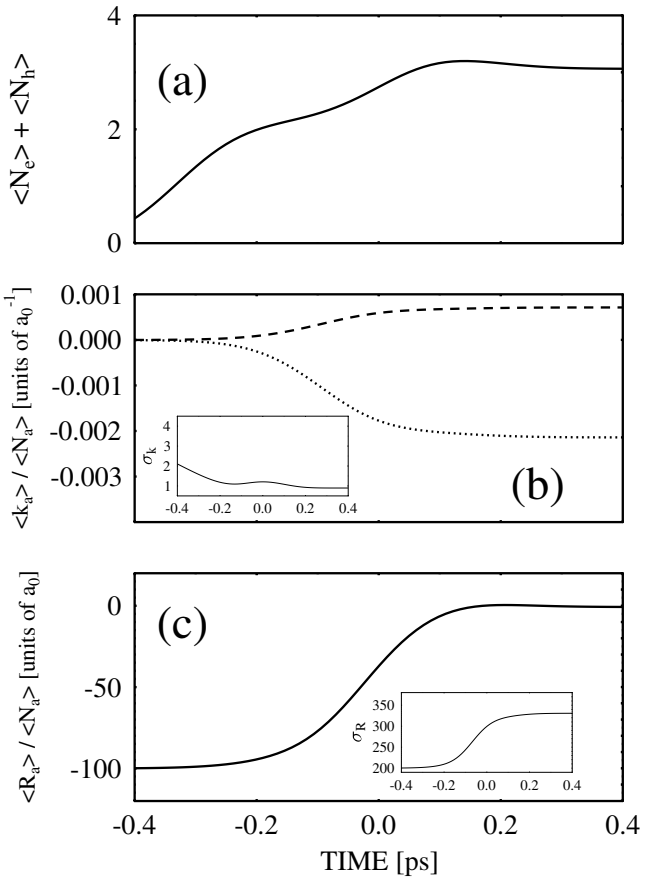

Figure 10. (a) Temporal evolution of the total particle number. (b) Temporal evolution of the wavevector per particle for electrons (dashed curve) and holes (dotted curve). The inset shows the variance (=width) of the corresponding momentum distributions in units of a_0^{-1}, which is identical for electrons and holes. (c) Temporal evolution of the spatial expectation value for electrons (dashed curve) and holes (dotted curve). The inset shows the variance (=width) of the corresponding spatial distributions in units of a_0, which is identical for electrons and holes. The results in this figure follow from the same calculation as used in figure 8.

For an analytical estimate we assume that the populations do not change during the pulse. Naturally neglecting the absorption is not quantitatively correct but gives us an idea what happens in the system. We also assume that the initial carrier distributions are symmetric in $\vec{K}$ i.e. there is no net momentum initially. Consequently the second term is equal to zero. We assume an initial Gaussian distribution where the spatial width is equal to R_i, of the order of the wavelength of the light (of the previous pulse) and the momentum width equal to $\hbar K_i$, of the order of inverse of the Bohr radius,

$$W_e^{init}(\vec{R}, \vec{K}) = w_{eo} \mathrm{e}^{-(\vec{R}-\vec{r}_o)^2/R_i^2} \mathrm{e}^{-\vec{K}^2/K_i^2} \tag{20}$$

where $\vec{r}_o$ is the vector pointing at the spatial maximum of the initial carrier distribution. The typical momentum width of the 1s-exciton excitation is of the order of an inverse Bohr radius. It is very difficult to create distributions with smaller momentum widths. There seems to be no *a priori* restriction to the constant w_{eo}. We also assume the light field to have a Gaussian

transverse profile with a transversal width of R_l, i.e. $|\vec{\mu}\cdot\vec{E}(\vec{R})|^2 = I_o(t)\mathrm{e}^{-\vec{R}^2/R_l^2}$. With these assumptions we obtain the total transverse momentum per carrier transferred from the light field to the carriers, defined as $\langle\Delta\vec{K}_e\rangle \equiv (\langle\vec{K}_e\rangle_{t=\infty} - \langle\vec{K}_e\rangle_{t=-\infty})/N_{tot}(t=\infty)$, to be given by

$$\langle\Delta\vec{K}_e\rangle \approx \int \mathrm{d}t\, I_o(t)\frac{2\Delta}{\gamma^2+\Delta^2}\vec{r}_o\frac{R_l^D}{(R_i^2+R_l^2)^{1+D/2}}\exp\left(-\frac{\vec{r}_o^{\,2}}{R_i^2+R_l^2}\right). \tag{21}$$

Assuming $R_i \approx R_l$, the maximum effect is obtained if $|\vec{r}_o| \approx R_l$. We see that for large detunings the momentum gained is of the order of $\frac{\int \mathrm{d}t\, I_o(t)}{\Delta R_l}$. In general the expression can take arbitrary values, but for the approximations made to hold, the expression is of the order of or less than $1/R_l$ which also is of the same order as the transversal momentum width of the chosen light beam with a Gaussian transversal profile. The result is the same for the holes. Hence, the wavelength of the light essentially determines how much momentum per particle the carrier system can absorb.

As we saw in the previous section, the initial carrier distribution disperses ballistically and is flattened out. This occurs in a time period of the order of $m_c R_i/\hbar K_i$. In this time a typical extra momentum $\hbar/R_l$ leads to an extra distance travelled of the order of $R_i/R_l K_i$. The width of the momentum distribution is typically of the order of an inverse Bohr radius which is a large quantity compared to the inverse wavelength. However the large momenta are connected to the internal motion of the exciton and the momenta connected to centre of mass motion are only of the order of the inverse wavelength. In a ballistic motion the internal degrees of freedom do not mix with the centre of mass motion of the electron–hole pairs. If the exciton system is created with a light beam having a Gaussian transverse profile and a frequency resonant with the 1s-exciton transition, the resulting system is in a Gaussian wavepacket for the centre of mass state but in a 1s-eigenstate for the internal state. In the following ballistic motion only the centre of mass state disperses because it is a superposition of eigenstates whereas the internal state is unchanged because it is an eigenstate. The momenta related to the dispersion are of the order of the inverse wavelength. Therefore we choose in our simulation $1/K_i$ to be of the order of the inverse wavelength. Because R_l is of the order of the wavelength of the light the travelled distance is of the same order of magnitude as the spatial width of the distribution. Hence, it should in principle be possible to detect the spatial deformations before the distribution has been flattened out. An additional difficulty is the fact that new carriers are created by the beam applying the force. These new carriers do not get net momentum but they will partially mask the changes in the initial momentum distribution. As a consequence, the momentum per particle will also be smaller.

In general, we conclude that one can optimize the light-force effect in a semiconductor by choosing short-wavelength light (which requires a large-gap semiconductor material), and an initial distribution that is highly localized.

5.2. Coulomb effects and weak intensity approximations

In the previous section, we have seen that a spatially inhomogeneous light field can exert a force on an electron–hole plasma in a semiconductor. This force is similar to the case of atoms exposed to spatially inhomogeneous light beams. However, we found that the effect in a semiconductor is less pronounced than in atoms, mainly because of the many-particle aspects of the plasma kinetics and the limitations in the observation time caused by the lifetime of the plasma. The question arises as to what aspects of our results are limited to electron–hole plasmas without Coulomb interaction. While it is clear that the lifetime issue is not strongly affected by our approximation of non-interacting electrons and holes, the details of the kinetic evolution could be strongly affected if the Coulomb interaction is included. Specifically, it

could be that the bound electron–hole pairs (excitons) experience light forces much more strongly than free electron–hole pairs.

In this subsection, we will show that the basic conclusions about the magnitude of the light force in semiconductors still hold if excitons rather than free electron–hole pairs are being accelerated by light. Of course, the general description of light forces on Coulomb-correlated electrons and holes is an extremely complex issue, and is not within the scope of this paper. A separate publication dealing with light forces on excitons will be published elsewhere [23]. In the following, we only summarize a few results for exciton systems in order to show that the basic conclusions about light forces in semiconductors discussed above are not artefacts of the non-interacting particle approximation.

Since the case with Coulomb interaction is generally not solvable, we concentrate here on a weak field approximation. In other words, we assume the light field to only yield the lowest-order optical nonlinearity, a so-called $\chi(3)$ response. Within this nonlinear optical regime, it has been shown that all Coulomb correlations can be treated exactly (dynamics-controlled trunction (DCT) formalism, [24]), if the initial electron–hole density is zero. Because of the requirement of vanishing initial population, we can apply this formalism in a strict sense only to the two-beam configuration similar to the discussion of figures 8–10 in section 4. The derivations of the following results will be presented in [23].

For an arbitrary light field which could, for example, consist of the two pulses used in figures 8–10, one finds that the total momenta for the carriers in lowest order in field strength are given by

$$\begin{aligned}\langle\vec{P}_e\rangle &= \frac{\hbar m_e}{M}\sum_{\vec{K},n}\vec{K}\,|u_{n00}(0)|^2\left|V\int_{-\infty}^{\infty}\mathrm{d}t\,\mathrm{e}^{\mathrm{i}\epsilon_{\vec{K}n00}t}\vec{\mu}\cdot\tilde{\vec{E}}(\vec{K},t)\right|^2\\ \langle\vec{P}_h\rangle &= \frac{\hbar m_h}{M}\sum_{\vec{K},n}\vec{K}\,|u_{n00}(0)|^2\left|V\int_{-\infty}^{\infty}\mathrm{d}t\,\mathrm{e}^{\mathrm{i}\epsilon_{\vec{K}n00}t}\vec{\mu}\cdot\tilde{\vec{E}}(\vec{K},t)\right|^2\end{aligned} \tag{22}$$

where M is the total mass of the exciton and $u_{n00}(0)$ is the wavefunction describing the relative motion of the ns exciton taken at the origin of the relative coordinate. We denote by $\epsilon_{\vec{K}n00}$ the energy, relative to the field frequency, of the ns exciton with centre of mass momentum $\vec{K}$. The expressions show that the total momentum is non-zero whereas the total current density $\langle\vec{J}_e\rangle+\langle\vec{J}_h\rangle=(e/m_e)\langle\vec{P}_e\rangle-(e/m_h)\langle\vec{P}_h\rangle=0$ is zero. The conclusion is that without dephasing or scattering processes a light field cannot cause a current proportional to the intensity. This, of course does not apply to the total momentum. For large fields this analysis is no longer applicable and that problem, along with a detailed derivation of equations (22), will be addressed in a separate publication [23].

Again, the weak field analysis above applies to all field configurations. To illustrate the consequences of the results we focus now on the case with two parallel beams. We assume two light pulses with equal Gaussian transversal profiles propagating in parallel spatially separated by distance r_o and otherwise equal pulse shapes except with a time delay τ between them. The total momentum per created pair, i.e, $(\langle\vec{P}_e\rangle+\langle\vec{P}_h\rangle)N$ where N is the total number of electron–hole pairs created by the light,

$$N=\sum_{\vec{K},n}|u_{n00}(0)|^2\left|V\int_{-\infty}^{\infty}\mathrm{d}t\,\mathrm{e}^{\mathrm{i}\epsilon_{\vec{K}n00}t}\vec{\mu}\cdot\tilde{\vec{E}}(\vec{K},t)\right|^2 \tag{23}$$

is given by

$$\langle\Delta\vec{K}\rangle\approx-\frac{\vec{r}_o}{2R_l^2}\frac{\exp\left(-\frac{\vec{r}_o^2}{4R_l^2}\right)\sin(\omega\tau)}{1+\exp\left(-\frac{\vec{r}_o^2}{4R_l^2}\right)\cos(\omega\tau)} \tag{24}$$

where ω is the centre frequency of the light beams.

We see that in the weak intensity limit the momentum transfer per pair is also independent of the intensity used. A finite time delay is necessary in order to have a net momentum created. This result can also be interpreted such that each of the two beams creates transversal forces with which they influence the carriers created by the other beam. The symmetry of the situation is broken by the time delay between the pulses leading to an absorption of net momentum. Finally, we note that maximally, the average momentum per pair created is again of the order of $1/R_l$. This coincides with our conclusion drawn above for the case without Coulomb interaction. In other words, excitonic effects do not change the order of magnitude of the light force.

6. Summary

In this paper we have studied the effects of the transversal light force in semiconductors. We have shown theoretically, using both analytical and numerical evaluations, that such a force, well known from atomic systems, indeed also exists in semiconductors.

Specifically, we have shown that a previously created carrier distribution without net momentum gets a net momentum when a light beam with a transverse intensity profile is applied close to it. The net momentum causes a spatial displacement of the carrier distribution, but for weak fields there is no net current related to this motion. We also showed that two parallel beams with suitably chosen time delays and spatial separations can be used to create a carrier distribution which has a net momentum and is therefore moving. We have found outlined fundamental differences between light forces in semiconductor and light forces in atomic systems, such as transient electron–hole excitation due to the light beam that exerts the force on, for example, pre-existing electron–hole pairs.

The main purpose of this study was to lay a theoretical foundation for transverse light forces in semiconductors. We have concentrated on light forces on electron–hole plasmas (free electron–hole pairs), but we have also found that light beams can exert transverse forces on excitons (bound electron–hole pairs). Further studies are needed in order to gain a better understanding of the role of Coulomb interactions (both in electron–hole plasmas and in exciton gases) and the role of phonons in the light-induced transverse quantum kinetics in semiconductors.

Acknowledgments

This work is supported by the Academy of Finland (hanke 48740), NSF (DMR-9972195), JSOP, COEDIP (University of Arizona) and a grant for CPU time at CCIT (University of Arizona).

References

[1] Mysyrowicz A, Hulin D, Antonetti A, Migus A, Masselink W T and Morkoc H 1986 *Phys. Rev. Lett.* **56** 2748
[2] von Lehmen A, Chemla D S, Zucker G E and Heritage J P 1986 *Opt. Lett.* **11** 609
[3] Fluegel B, Peyghambarian N, Lindberg M, Koch S W, Joffre M, Hulin D, Migus A and Antonetti A 1987 *Phys. Rev. Lett.* **59** 2588
[4] Becker P C, Fragnito H L, Cruz C H B, Fork R L, Cunningham J E, Henry J E and Shank C V 1988 *Phys. Rev. Lett.* **61** 1647
[5] Chemla D S, Know W H, Miller D A B, Schmitt-Rink S, Stark J B and Zimmermann R 1989 *J. Lumin.* **44** 233
[6] Hulin D and Joffre M 1990 *Phys. Rev. Lett.* **65** 3425
[7] Webb M D, Cundiff S T and Steel D G 1991 *Phys. Rev. Lett.* **66** 934

[8] Cundiff S T, Knorr A, Feldmann J, Koch S W, Göbel E O and Nickle H 1994 *Phys. Rev. Lett.* **73** 1178
[9] Schneider H and Ploog K 1994 *Phys. Rev.* B **49** 17050
[10] Saiki T, Kuwata-Gonokami M, Matsustue T and Sakaki H 1994 *Phys. Rev.* B **49** 7817
[11] Fürst C, Leitenstorfer A, Nutsch A, Tränkle G and Zrenner Z 1997 *Phys. Status Solidi* b **204** 20
[12] Giessen H, Knorr A, Haas S, Koch S W, Linden S, Kuhl J, Hetterich M, Gruen M and Klingshirn C 1998 *Phys. Rev. Lett.* **81** 4260
[13] Schülzgen A, Binder R, Donovan M, Lindberg M, Wundke K, Gibbs H, Kithrova G and Peyghambarian N 1999 *Phys. Rev. Lett.* **82** 2346
[14] Sieh C, Meier T, Jahnke F, Knorr A, Koch S W, Brick P, Hübner M, Ell C, Prineas J, Khitrova G and Gibbs H 1999 *Phys. Rev. Lett.* **82** 3112
[15] Shah J 1996 *Ultrafast Spectroscopy of Semiconductors and Semiconductor Nanostructures (Springer Series in Solid-State Sciences vol 115)* (Berlin: Springer)
[16] Ashkin A 1970 *Phys. Rev. Lett.* **25** 156
[17] Kasantsev A, Surdutovich G and Yakovlev V 1990 *Mechanical Action of Light on Atoms* (Singapore: World Scientific)
[18] Cohen-Tannoudji C 1992 *Fundamental Systems in Quantum Optics (Les Houches Session LIII)* ed J Dalibard, J Raimond and J Zinn-Justin (Amsterdam: Elsevier)
[19] Meystre P 2001 *Atomic Optic* (New York: Springer)
[20] Schäfer W and Treusch J 1986 *Z. Phys.* B **63** 407
[21] Henneberger K and Haug H 1988 *Phys. Rev.* B **38** 9759
[22] Knorr A, Steiniger F, Girndt A, Stroucken T, Haas S, Thomas P and Koch S W 1995 *Nuovo Cimento* D **17** 1265
[23] Lindberg M and Binder R 2003 at press
[24] Axt V M and Stahl A 1994 *Z. Phys.* B **93** 195